

Gyro in the Air: Tracking 3D Orientation of Batteryless Internet-of-Things

Teng Wei and Xinyu Zhang
Department of Electrical and Computer Engineering
University of Wisconsin - Madison
twei7@wisc.edu, xyzhang@ece.wisc.edu

ABSTRACT

3D orientation tracking is an essential ingredient for many Internet-of-Things applications. Yet existing orientation tracking systems commonly require motion sensors that are only available on battery-powered devices. In this paper, we propose Tagyro, which attaches an array of passive RFID tags as orientation sensors on everyday objects. Tagyro uses a closed-form model to transform the runtime phase offsets between tags into orientation angle. To enable orientation tracking in 3D space, we found the key challenge lies in the imperfect radiation pattern of practical tags, caused by the antenna polarity, non-isotropic emission and electromagnetic coupling, which substantially distort phase measurement. We address these challenges by designing a set of phase sampling and recovery algorithms, which together enable reliable orientation sensing with 3 degrees of freedom. We have implemented a real-time version of Tagyro on a commodity RFID system. Our experiments show that Tagyro can track the 3D orientation of passive objects with a small error of 4° , at a processing rate of 37.7 samples per second.

CCS Concepts

•Human-centered computing → Ubiquitous computing; Ambient intelligence; •Hardware → Digital signal processing; Beam-forming; Sensors and actuators; Sensor devices and platforms;

Keywords

Wireless Sensing; Orientation Tracking; Internet-of-Things; RFID; Tag Array; Coupling Effect

1. INTRODUCTION

3D orientation is an essential input to many pervasive applications, such as motion tracking [1], mobile gaming, and activity recognition [2]. However, existing orientation tracking systems commonly require motion sensors like gyroscope and compass, which are only available on battery-powered devices. Tracking the orientation of passive batteryless objects is an equally important but more challenging problem.

Permission to make digital or hard copies of all or part of this work for personal or classroom use is granted without fee provided that copies are not made or distributed for profit or commercial advantage and that copies bear this notice and the full citation on the first page. Copyrights for components of this work owned by others than ACM must be honored. Abstracting with credit is permitted. To copy otherwise, or republish, to post on servers or to redistribute to lists, requires prior specific permission and/or a fee. Request permissions from permissions@acm.org.

MobiCom'16, October 03-07, 2016, New York City, NY, USA

© 2016 ACM. ISBN 978-1-4503-4226-1/16/10...\$15.00

DOI: <http://dx.doi.org/10.1145/2973750.2973761>

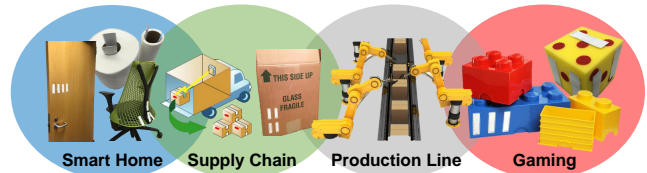


Figure 1: Applications of passive orientation sensing in IoT.

A passive orientation sensing system can enable many new Internet-of-Things (IoT) applications (Figure 1). For example, in smart-home environment, it can monitor the rotation and placement of daily objects (e.g., detecting door closure and monitoring activity of a rolling chair). In a supply chain, it can detect the tilt angle of orientation-sensitive cargo and warn the human workers when necessary. Orientation information of products on a conveyor belt can assist robotic arms to pick up an item using proper posture. Likewise, there exist numerous applications in mobile gaming (e.g., guiding the positioning of LEGO pieces) and library management (e.g., detecting upside down books). Existing passive orientation tracking solutions are predominantly based on computer vision [3–7]. Such systems often require extensive per-object per-angle training. They are sensitive to background variation, ambient light condition, and occlusion. Therefore, they are unsuitable for ad-hoc IoT applications.

In this paper, we propose Tagyro, which can track the 3D orientation of passive objects using RFID tags. The basic idea is to attach multiple tags to different spots on the object, which constitute a tag array. Some example array patterns are illustrated in Figure 2. An RFID reader can measure the tag phase, i.e., the phase of signals returned from each tag. When the tag array rotates together with the object, the tag-to-reader distance among different tags varies, which in turn affects the relative phase offset between tags (referred to as phase difference of arrival or PDoA). Tagyro builds a closed-form model that transforms the measured PDoA into an orientation spectrum, which characterizes the likelihood of each orientation angle. It then derives the tag array's 2D orientation from the peak of orientation spectrum. By attaching an additional RFID antenna and tag array, Tagyro can aggregate the outputs from multiple 2D estimators and produce a 3D orientation estimation for the target object.

Realizing such an RFID-based 3D orientation tracking entails three key challenges that are unaddressed in previous RFID sensing systems [8–12]. First, to prevent phase ambiguity, adjacent tags in a tag array must be placed within close proximity. However, our experiments reveal that the closely-placed tags tend to alter each other's phases due to sophisticated electromagnetic interactions. Such coupling effect deviates the phase value from the traditional phase-distance model [8]. To address this issue, we propose an Array Layout Sensing (ALS) algorithm, which approxi-

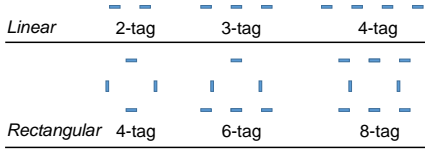


Figure 2: Examples of linear and square tag arrays from the top view (showing cross sections of tags).

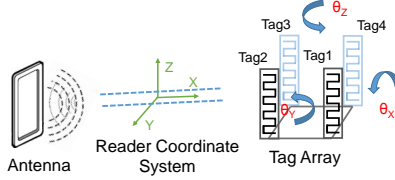


Figure 3: Coordinate system refers to the reader antenna. Tag orientation is defined as the rotation offset ($\theta_x, \theta_y, \theta_z$) along each axis.

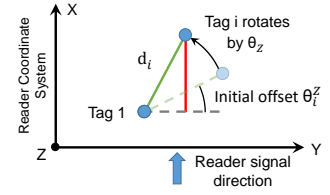


Figure 4: Relation between the tags' PDoA and rotation angle. This example shows rotation along the Z-axis (by projecting to the X-Y plane).

mately models the coupling effect as if the tags repel each other in the physical space. ALS also enables Tagyro to automatically sense the tag array's effective layout – a critical input for the orientation spectrum computation. Consequently, ALS also frees the user from knowing the array's physical layout or placing the array with precise geometry.

Second, the radiation pattern of a practical RFID tag is far from the ideal isotropic model, *i.e.*, a point source that scatters signals uniformly in 3D space. Instead, it has blind directions with extremely weak emissions, rendering phase measurement infeasible. Tagyro addresses this challenge using a dual-array setup, where two arrays are arranged in orthogonal angles to compensate the blind directions. Tagyro can single out valid phase readings, and then unify the results to estimate the object's orientation with 3 degrees-of-freedom (DoF).

Third, commercial FCC-compliant RFID readers run in the frequency-hopping mode and interrogate the tags sequentially, which cause phase discontinuity and significantly slow down the orientation sensing. We design a simple per-reader phase calibration mechanism, along with phase interpolation, which improves the phase-reading precision/granularity.

Tagyro, to our knowledge, represents the first wireless sensing system that can track the 3D orientation of passive objects. Its contributions can be summarized as follows.

(i) We propose an RFID tag-array setup for phase-based orientation tracking, and empirically study the impact of tags' imperfect radiation patterns on phase reading. Our study reveals how the tag polarity, blind direction and coupling effect distort phase measurement, which has not been reported by previous RFID sensing/localization systems [8–14].

(ii) We propose an innovative algorithm to sense the effective layout of a tag array, which overcomes the tag coupling effect. We further propose mechanisms to combat the tags' non-isotropic radiation patterns, enabling orientation sensing in 3D space without blind direction. We have also developed phase calibration mechanisms and enabled fast orientation sensing on standard-compliant RFID devices.

(iii) We implement Tagyro on a COTS RFID system as a real-time 3D orientation sensing framework. Our experimental results show that Tagyro can track the 3-DoF orientation of an object at an average accuracy of 4° , with processing rate >37.7 samples/second and response latency <0.75 seconds. Tagyro achieves comparable accuracy and sampling rate as state-of-the-art gyroscope-based systems [15], but it needs no battery on the object, and evades the notorious drifting issue.

2. PRELIMINARIES

2.1 Phase Model for an RFID System

An RFID reader can transmit continuous-wave signals to interrogate a tag, and then receive backscattered signals from the tag

which contains its unique identity information. The phase offset between the transmitted and received signals depends on the round-trip propagation distance d , as well as hardware-specific factors. Following a standard phase-distance model [8, 16], the phase value ϕ , also referred to as *tag phase*, equals:

$$\phi = \text{mod}\left(\frac{2\pi d}{\lambda} + \phi_{\text{Reader}} + \phi_{\text{Tag}}, 2\pi\right), \quad (1)$$

where λ denotes the signal wavelength, and ϕ_{Reader} and ϕ_{Tag} are the additional phase offsets induced by the reader's transmission/receiving circuits and tag's antenna response. Eq. (1) implies that a single tag is insufficient for 3D orientation sensing, because simply changing the tag's orientation may not change the distance d and the phase ϕ .

2.2 Phase Difference of Arrival of a Tag Array

The basic idea of our approach is to form a tag array with multiple tags. Due to different distances to the reader, the tags cause different phase offsets, which we call the *Phase Difference of Arrival* (PDoA). Rotation of the tag array results in different PDoA values, from which we can estimate the orientation of the tag array, and hence the orientation of the object it is attached to.

Consider Figure 3 where 4 tags form a square array. We first specify a 3D *coordinate system for the RFID reader*, in which the X-axis is parallel to the direction from the reader to the center of the tag array, and the X-Y plane is parallel to the ground. The *tag array's orientation* is defined as the rotation offset ($\theta_x, \theta_y, \theta_z$) along each axis, relative to an initial state specified by the user. *This coordinate system allows us to track the tag array's orientation from the reader antenna's perspective*. Note that Tagyro is different from active motion sensors (gyroscope and magnetometer) [15], since the coordinate system will change *w.r.t.* to the position of the tag array. On the other hand, active motion sensors are location-independent because gravitational and magnetic fields on earth are used as the reference coordinate.

Figure 4 illustrates the rotation around the Z-axis by projecting 3D space on to the X-Y plane. In this example, signals first reach tag 1 before tag i , and thus PDoA (tag i to tag 1) is positive. More generally, *the direction and amount of rotation determine the sign and value of PDoA, respectively*. Assuming signals come from far field, the PDoA $\Delta\phi_i$ for any tag i to the reference tag, say tag 1, can be derived from the tag separation distance projected to the reader's signal direction (*i.e.*, the red line in Figure 4):

$$\begin{aligned} \Delta\phi_i(\theta_Y, \theta_Z, d_i) &= \phi_i - \phi_1 \\ &= \text{mod}\left(\frac{4\pi d_i \sin(\theta_Y + \theta_Y^i) \sin(\theta_Z + \theta_Z^i)}{\lambda} + \Delta\phi_{\text{Tag}}^i, 2\pi\right), \quad (2) \end{aligned}$$

where d_i is the distance between the i^{th} and reference tag. θ_Y^i and θ_Z^i are initial angular offsets for tag i and reference tag in the initial state, which gauge the rotations along Y and Z axes respectively *w.r.t.* the directions of zero PDoA. They can be calculated from the array geometrical layout (to be addressed in Sec. 4.3). $\Delta\phi_{\text{Tag}}^i$ is

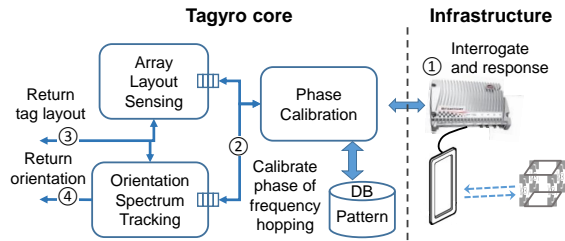


Figure 5: Tagyro’s Architecture and operation workflow.

the difference of antenna phase response (cf. Sec. 2.1) between tag i and the reference tag, which will be calibrated and removed by our array sensing module (Sec. 4.3.3). Note that PDoA cancels the unknown phase offset ϕ_{Reader} introduced by the reader’s circuits.

In addition, note that the PDoA is irrelevant to the X-axis rotation in this example setup (Figure 3), since any rotation along X-axis does not change the distance offset between different tags and the reader. Therefore, a single reader antenna can only track the array rotation with 2 Degree-of-Freedom (DoFs), i.e., along Y and Z axes. For 3-DoF tracking, Tagyro requires a reader with at least 2 antennas, which will be discussed in Sec. 4.4.

3. Tagyro OPERATION

Tagyro is an orientation sensing system that generalizes the aforementioned ideal PDoA tracking. To use Tagyro, a user needs to attach an array of RFID tags on the target object, following certain empirical guidelines and without knowing the precise geometrical relation between tags.

Figure 5 illustrates Tagyro’s flow of operations, comprised of the following steps: (1) The reader interrogates the tag array following standard EPC protocol [17], which reads the tags sequentially and resolves collision via retransmission. Commercial readers (e.g., the Impinj R420 [18] that we use) can extract many pieces of information such as tag ID, phase and Received Signal Strength Indicator (RSSI), which are forwarded to a PC host running Tagyro. (2) Tagyro’s *phase calibration* module pre-processes the phase information, and removes the phase discontinuity caused by the reader’s channel hopping. (3) Tagyro’s *Array Layout Sensing* (ALS) module estimates the tag array’s effective layout, which differs from the geometrical layout due to mutual coupling between tags. (4) Given the tag array layout, Tagyro measures the tag phase and runs an *orientation-spectrum tracking mechanism* to continuously track the tag array’s orientation.

In what follows, we describe Tagyro’s major design components and algorithms. We first describe how to compute orientation from the PDoA, assuming the tag array’s layout is known (§ 4.1). Second, we explore the main challenges in PDoA and tag layout estimation (§ 4.2), particularly caused by the tags’ imperfect radiation pattern. We introduce the ALS algorithm that estimates the tag array’s effective layout, taking into account the coupling effect (§ 4.3). Third, we extend the single-array and single-antenna reader case to dual-array and dual-antenna reader, in order to realize 3-DoF orientation tracking (§ 4.4). We will also discuss phase calibration and run-time optimization mechanisms that improve the accuracy and speed of phase reading (§ 4.5 and § 4.6).

4. DESIGN

4.1 Tracking through Orientation Spectrum

We first focus on the 2-DoF orientation, i.e., sensing (θ_Y, θ_Z) , the array’s angular rotation along Y and Z axis, relative to its initial state. Given the measured PDoA between each tag i and the

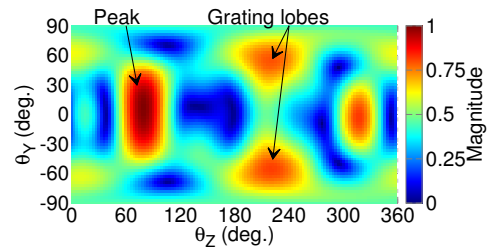


Figure 6: Example orientation spectrum from measurement.

reference tag, Tagyro estimates the tag array’s orientation by computing an *orientation spectrum* – a 2D intensity graph in which each pixel indicates the likelihood of an orientation. We use the phaser-domain difference between the theoretical PDoA $\Delta\Phi_i$ (computed from Eq. (2)) and measured PDoA $\Delta\hat{\Phi}_i$ as pixel intensity, i.e.,

$$I(\theta_Y, \theta_Z) = \left| \sum_{i=1}^K e^{j(\Delta\Phi_i(\theta_Y, \theta_Z, d_i) - \Delta\hat{\Phi}_i)} \right| / K \quad (3)$$

where K is the tag number in the array. The phaser domain operation inherently handles the phase aliasing. When the theoretical PDoA matches the measured value, e.g., $|\Delta\Phi_i - \Delta\hat{\Phi}_i| \approx 0$ for all i , the pixel will have the maximum intensity equal to 1. Otherwise the pixel intensity will be close to 0. The complexity of computing the spectrum is $O(N^2)$, where N is the number of values for each DoF rotation. In Tagyro, we discretize the rotation value θ_Y and θ_Z into 3° granularity, resulting in an orientation spectrum with 120×120 pixels.

The 2-DoF orientation is estimated by finding the highest peak in the orientation spectrum:

$$\{\theta_Y, \theta_Z\} = \arg \max_{\theta_Y \in [0, 2\pi), \theta_Z \in [0, 2\pi)} I(\theta_Y, \theta_Z). \quad (4)$$

Taking the 4-tag square array in Figure 3 again as an example, where neighboring tags are separated by the quarter wavelength of 8.2 cm, Figure 6 plots the orientation spectrum when the array rotates at $(\theta_Y = 0^\circ, \theta_Z = 80^\circ)$. The highest peak position occurs exactly at the same orientation. Besides, there are weaker grating lobes that are caused by the *spatial ambiguity* effect.

Spatial ambiguity is a well known effect when using multi-antenna to estimate a signal’s angle of arrival – multiple angles may have similar likelihood of estimation. To minimize the spatial ambiguity, antennas need to be separated by less than half-wavelength ($\lambda/2$) away. For an RFID tag array, the equivalent separation should be $\lambda/4$ (i.e., 8.2 cm for 915 MHz UHF tags), because the signals traverse a round-trip propagation. Though grating lobes are generally weaker than the main lobe, they may occasionally obscure the detection of true peak because of residual phase measurement error and noise in RF channel. To ensure the robustness of Tagyro, instead of picking a single strongest peak, we search for the top three peaks in the orientation spectrum, and take the one that is closest to the previous estimation as final orientation result. This serves as a simple moving average outlier filter.

The above ideal orientation-spectrum tracking model requires three underlying conditions: (i) a tag backscatters wireless signals like an isotropic point source, so the signals cover 3D space without blind direction; (ii) the phase reading of a tag follows a predictable model over distance (Eq. (1)); (iii) tag array’s relative layout and the corresponding IDs are known. We next explore the practical challenges and solutions in Tagyro to meet these conditions.

4.2 Impact of Tag Radiation Pattern

We conduct empirical studies using a COTS RFID platform (Impinj R420 [18]) to better understand the radiation property of RFID

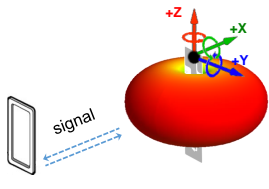


Figure 7: Measuring RSS and phase of a tag rotating along each axis. The 3D heat map shows radiation pattern of a typical tag.

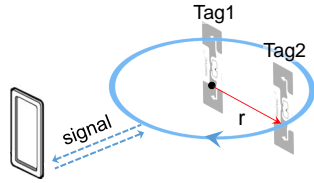


Figure 8: Measuring the PDoA of a two-tag array. One tag is in the rotation center and the other rotates along a circle $r = 6cm$.

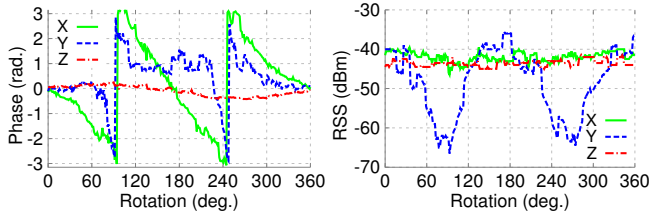


Figure 9: Measured phase (left) and RSS (right) of a single tag rotating along each of the three axes respectively.

tags. Although the first two of above basic assumptions (about RSS and phase) have been applied in previous works to localize tags in a 2D space [8, 19, 20], we are particularly interested in verifying whether they still hold under the tag array setup and the implications for 3D orientation tracking.

4.2.1 Rotation of a Single Tag – Polarity and Blind Direction Issues

Observation 1 *The phase of a single tag is not only determined by the distance, but also affected by its relative orientation to the reader antenna.*

We first reinvestigate the standard phase-distance model (Eq. 1) under varying tag orientations. We place a slim tag 1.5 m in front of a flat-panel reader antenna (Figure 7), and rotate the tag center along each axis. Figure 9 plots the corresponding phase change. Ideally, the phase should remain constant, if it only depends on the tag-to-reader distance. Surprisingly, we find that the phase shifts linearly with the rotation along X-axis, and abrupt phase jumps occur with rotation along Y-axis. The phase only remains unchanged for the rotation along Z-axis.

This phenomenon is caused by the *polarity* of RFID antennas. Due to form-factor constraint, a tag’s antenna is commonly designed as a dipole, which is linear-polarized along the tag body (*i.e.*, Z-axis in Figure 7). On the other hand, to ensure they can read tags from a variety of angles, most RFID readers’ antennas are circular-polarized [21] – They comprise two perpendicular dipoles, fed with signals of 90° phase difference. When the tag rotates along the X-axis by 90° , the phase of signal received by the tag will change by $\frac{\pi}{2}$. *Since the signals traverse a round-trip propagation back to the reader, the corresponding phase shift measured by the reader doubles.* Similarly, the tag phase jump of 2π when rotating around Y-axis by 180° is also due to the abrupt change of polarity direction. We repeat the experiment using other types of tags (Sec. 5) and observe a similar result.

Implication: Antenna polarity affects the tag phase, and may confuse the orientation spectrum computation which assumes phase only depends on the tag-to-reader distance. *To isolate the polarity effect, in Tagyro, we enforce a constraint on the tag placement, called polarity alignment – within a tag array, the tags’ bodies must be parallel to each other.* In this way, polarity introduces the

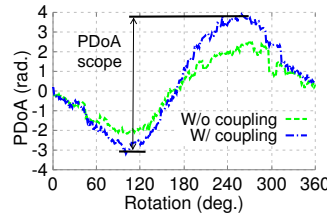


Figure 10: Measured PDoA value of a two-tag array.

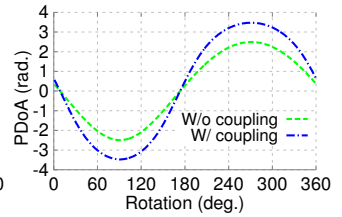


Figure 11: Simulated PDoA value of a two-tag array.

same phase shift among all tags during rotation, and does not affect PDoA.

Observation 2 *An RFID tag has non-isotropic radiation: it mainly backscatters signals surrounding the tag body (XY-plane in Figure 7), and has blind direction along its radial direction (Z-axis).*

Under the same setup as above, Figure 9 plots the RSS with different tag rotations. We see that the tag reflects consistently strong RSS when rotating around X or Z axis. Yet, if it rotates around Y-axis, the RSS drops significantly (by 20 dB) when the tag’s radial direction points to the reader. The reader cannot reliably decode the tag’s signal at such blind direction, and hence the phase measurement becomes erroneous.

Implication: The blind direction of an RFID tag limits the range of orientation that Tagyro can track using a single tag array. To realize 3D orientation sensing, the blind direction of RFID tags must be compensated by other means.

4.2.2 Rotation of a Tag Array – Coupling Between Tags

Observation 3 *The phase of each tag in the tag array will be affected by neighboring tags through the coupling effect, which deviates actual PDoA from the standard phase-orientation model (Eq. 2).*

The coupling effect of RFID tag occurs in near-field where signals backscattered from a responding tag generate resonant voltage in the antennas of other tags [22]. As a result, besides the signal from responding tag, other nearby tags will also emit signals, which further alters the phase received by the reader. We now conduct two experiments to quantify such effect.

We now create a two-tag array following the polarity alignment requirement, and measure the PDoA between them (Figure 8). One tag is in the rotation center and the other rotates along a circle of radius $r = 6cm$. To evaluate the PDoA without coupling effect, we also collect the phase trace by rotating only one tag (removing the other), and then compute the PDoA at each of the sampling locations along the circle.

Figure 10 plots the PDoA for cases with (w) and without (w/o) coupling effect. We observe that when there is no coupling, the measured PDoA matches the standard model (Eq. (2)). However, when two tags rotate together, the *PDoA scope*, *i.e.*, difference between maximum and minimum values, has increased significantly. The result shows that PDoA value is scaled by the coupling effect between tags.

To better understand the root cause of PDoA deviation, we model the coupling effect of two tags as illustrated in Figure 8. We first consider the case without coupling, the carrier signal backscattered from Tag1 to the RFID reader is characterized by:

$$s_1 = A_1 \exp(j2\pi \frac{2d_1}{\lambda}) \quad (5)$$

where A_1 denotes the amplitude of received signal and $2d_1$ is the round-trip distance between tag and reader. Without loss of generality, we omit other constant phase offsets caused by tag/reader

antennas. Eq. (5) is consistent with the standard phase-distance model (Eq. (1)) – phase is determined by the tag-to-reader distance.

When the coupling effect occurs, RFID reader essentially receives two copies of signals. One is the original signal coming from the responding tag, and the other copy is generated by the resonant voltage and coming from the other tag. Compared to the original one, the resonant copy experiences certain attenuation and phase shift, which are uniquely determined by the coupling coefficients between the two tags. We denote the resonant signal emitted from Tag2 as s_2^c , which is given by:

$$s_2^c = A_2^c \exp(j2\pi \frac{d_1 + d_2 + r}{\lambda} + \varphi^c) \quad (6)$$

where A_2^c and φ^c are the amplitude and phase offset of the resonant signal. d_2 and r are the Tag2-to-reader and Tag1-to-Tag2 distances respectively. In a similar way, when Tag2 is responding, we can model the signals from Tag1 and Tag2 as s_1^c and s_2 respectively.

When both copies of signals overlap and together reach the RFID reader, the measured phase value will deviate from the origin one, and thus the PDoA distorts. We plug in empirical parameters $A_1 = 1$, $A_2 = 0.5$, $\varphi^c = 90^\circ$, and simulate the PDoA of a two-tag array based on the analytical model. Figure 11 shows that the simulation result is highly consistent with our experimental measurement.

We further evaluate the extent of coupling effect over tag separation distance. We vary the radius r from 3cm to 18cm, at 3cm step. We use the PDoA deviation as metric, *i.e.*, the difference of PDoA scope relative to the case without coupling. Figure 12 shows that *the closer two tags are placed to each other, the stronger the PDoA deviation will be*. Recall that computing orientation spectrum requires tags to be placed within quarter-wavelength distance (8.2cm) to minimize the spatial ambiguity (Sec. 4.1). Yet at this separation, coupling effect is strong and unavoidable.

Implication: The coupling effect, which deviates PDoA value from the phase-orientation model, will compromise the peak of orientation spectrum and consequently affect the performance of rotation tracking.

In summary, the above experiments reveal that the radiation pattern of RFID tags is far from the ideal model, and may compromise any RSS/phase-based sensing algorithms in 3D space. We now present the countermeasures in Tagyro.

4.3 Combating Tag Coupling Effect

4.3.1 Effective Distance Between Tags

Since tag coupling distorts the phase and PDoA, a natural countermeasure is to model the coupling effect and compensate the distortion accordingly. However, such a model must capture the mutual impedance between tags [23], which depends on elusive factors (*e.g.*, antenna shape and material) that are unlikely to be available to end-users.

To address this issue, we make an important observation from Figure 10: under the coupling effect, the scope of PDoA is scaled, but the relation between rotation angle and PDoA maintains a similar trend as the no-coupling case. In other words, we can approximate the end-effect as virtually *rescaling* the tag separation to an appropriate value, which we call *effective distance*. Formally, the effective distance between the tag i and the reference tag is modeled as \hat{d}_i , which maximizes the alignment between measured PDoA and the theoretical value for any given orientation (θ_Y, θ_Z) :

$$\{\hat{d}_i, 1 \leq i \leq K\} = \arg \max_{d_i, 1 \leq i \leq K} \left| \sum_{i=1}^K e^{j(\Delta\Phi_i(\theta_Y, \theta_Z, d_i) - \Delta\hat{\Phi}_i)} \right|. \quad (7)$$

To verify this model, we conduct a benchmark experiment involving two tags with a physical distance of 6 cm. We measure

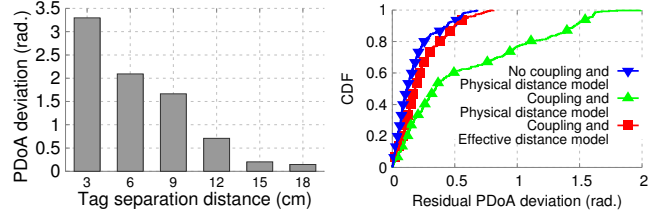


Figure 12: PDoA deviation over tag separation distance. **Figure 13: CDF of residual PDoA deviation. Physical distance and effective distance are 6 cm and 9 cm.**

the PDoA by rotating the array to three known orientations, and then find the effective distance through Eq. (7). Figure 13 shows the CDF of PDoA deviation. We can see that, compared with the physical distance model that does not account for coupling, effective distance model reduces the maximum PDoA estimation error from 2 radians to 0.7 radians, and mean to as small as 0.1 radians. Overall, PDoA deviation is reduced to an extent comparable to the case without coupling effect (*cf.* Sec. 4.2.2). Note that, even without coupling, the PDoA model is imperfect and has minor residual errors due to the multipath and RF noise [8–10, 13]. They will be incorporated in our system level experiments.

4.3.2 Sensing the Effective Layout of a Tag Array

However, in practice, it is difficult to compute the effective distance from Eq. (7) for more than two tags due to the huge search space. More importantly, Eq. (7) requires the knowledge of multiple rotation angles as input, which the user may not even be able to obtain. In Tagyro, we design an Array Layout Sensing (ALS) algorithm, which can automatically sense the effective distance between tags, and hence the layout of the entire tag array under coupling, which we refer to as *effective layout*.

First, to avoid requiring the knowledge of rotation angle, our key insight is that the scope of PDoA is determined by the effective distance of two coupled tags, and it is independent of the array’s orientation. The PDoA value is bounded within $[-\frac{4\pi\hat{d}}{\lambda} + \Delta\phi_{Tag}, \frac{4\pi\hat{d}}{\lambda} + \Delta\phi_{Tag}]$ (*cf.* Eq. (2)). Thus, the effective distance can be determined by the PDoA scope as:

$$\hat{d} = \frac{\lambda}{4} \frac{PDoA_scope}{2\pi}. \quad (8)$$

To obtain the *PDoA_scope*, Tagyro requires the user to rotate the tag array by more than one cycle (360°) roughly around each axis. Meanwhile, it measures the PDoA values and uses the difference between maximum and minimum PDoA as the *PDoA_scope*. This is a simple one-time calibration, needed only when the tag array is first formed.

Second, when measured phase value exceeds 2π , the RFID reader wraps it back to the $[0, 2\pi]$ range, which may cause ambiguity in estimating the max and min PDoA values. We remove the ambiguity through phase unwrapping [24]. Since the reader typically queries the tag at a much higher speed compared to the tag array rotation, the change between consecutive PDoA values is minor. Thus, any PDoA change greater than π or smaller than $-\pi$ indicates the occurrence of phase jumping, which can be removed by adding/subtracting π to the subsequent samples of PDoA values.

Third, computing the orientation spectrum requires the relative layout of tags instead of their separation. We approach this by mapping the tags’ pairwise effective distance to the entire tag array’s effective layout. This can be formulated as a Classical Multi-Dimensional Scaling (CMDS) problem [25], which takes a matrix

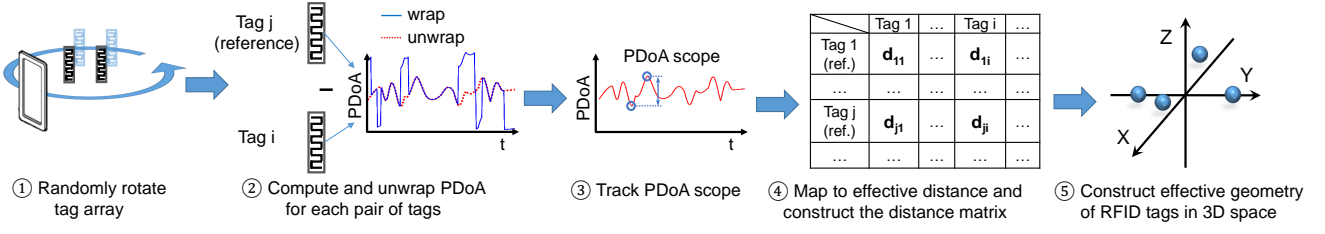


Figure 14: Array Layout Sensing (ALS) algorithm to sense the effective geometry of a tag array.

Algorithm 1 Sensing the effective layout of a tag array

```

1: global  $p[1 \times K] \leftarrow -1$  ▷ Vector of historical phase
2: global  $a[K \times K] \leftarrow 0$  ▷ Matrix of PDoA
3: global  $\mu[K \times K] \leftarrow -\text{inf}$  ▷ Matrix of maximum PDoA
4: global  $\nu[K \times K] \leftarrow \text{inf}$  ▷ Matrix of minimum PDoA
5: procedure SenseGeometry( $\sigma, \phi$ ) ▷  $\sigma$  tag ID,  $\phi$  phase
6:   if  $p[\sigma] == -1$  then ▷ Initialize new incoming tag
7:      $[p[\sigma], a[\sigma]] \leftarrow \text{initialize}(\phi)$ 
8:   end if
9:   for each tag  $i$  do ▷ Reference tag
10:     $a[\sigma][i] = \phi - p[i]$  ▷ Compute PDoA
11:     $a[i][\sigma] = p[i] - \phi$ 
12:     $\text{unwrap}(a)$  ▷ Phase unwrapping
13:    if  $a[\sigma][i] > \mu[\sigma][i]$  then ▷ Update max PDoA
14:       $\mu[\sigma][i] = a[\sigma][i]; \nu[i][\sigma] = a[i][\sigma]$ 
15:    end if
16:    if  $a[\sigma][i] < \nu[\sigma][i]$  then ▷ Update min PDoA
17:       $\nu[\sigma][i] = a[\sigma][i]; \mu[i][\sigma] = a[i][\sigma]$ 
18:    end if
19:  end for
20:   $\hat{d} \leftarrow \frac{\lambda}{4} \frac{\mu - \nu}{2\pi}$  ▷ Construct effective distance matrix
21:  return  $G \leftarrow \text{cmdscale}(\hat{d})$  ▷ CMDS to effective geometry
22: end procedure

```

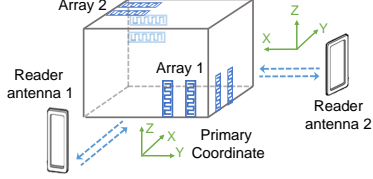


Figure 15: Example of dual-array, dual-antenna reader setup.

that describes dissimilarity between points (e.g., effective distance in our case) as input, and outputs a coordinate matrix in the geometrical space that minimizes the residual distance error. An approximate algorithm [26] can solve this problem efficiently at complexity $O(K \log K)$ for K tags. We apply the CMDS function built-in MATLAB which by default projects the K points into a K -dimensional space. Since tags are located in a 3-D space, the coordinate values for the higher $K - 3$ dimensions are small and close to zero. So we can take outcomes in the first 3 dimensions as tag coordinates and ignore the others without much loss of accuracy. It is worth noting that using other implementations of CMDS algorithm will not affect the key design of Tagyro.

Figure 14 summarizes the operations of Tagyro’s ALS algorithm: (i) When the array randomly rotates, ALS computes the PDoA from a reference tag to every other tags; (ii) The unwrapping operation removes the aliasing phase; (iii) Then ALS determines the scope of PDoA by tracking the max and min values of phase, and maps it to effective distance; (iv) The above steps are repeated for another reference tag until all pairwise effective distances are obtained, which together form a matrix; (v) Finally, Tagyro computes the effective tag layout from the effective distance matrix using the CMDS algorithm.

Algorithm 1 presents our real-time implementation of the ALS scheme in Tagyro. It takes the tag ID σ and phase ϕ as input, and updates the instant layout G to the user as the reader continuously queries the tag array. The algorithm can be stopped by user when the sensed array layout stabilizes.

We emphasize that a tag array’s effective layout may differ from the geometrical layout. The difference reflects the overall impact of the coupling effect. Figure 14 illustrates the output from a mi-

crobenchmark experiment, where we run ALS to sense a 4-tag square array. All 4 tags are physically placed on the X-Y plane, but in the effective layout, 2 of them are repelled from the plane, which account for the PDoA deviation due to coupling.

It is worth noting that ALS is a one-time procedure as long as the geometry layout of the tag array remains unchanged. If the effective layout can be measured at factory calibration time, then the ALS procedure can be skipped. In case when the tag-attached object is not suitable for rotation, the user can hold the RFID reader and scan around the object to complete the ALS.

4.3.3 Removing Tag’s Initial Phase Offset

The PDoA comprises $\Delta\phi_{\text{Tag}}$ – the difference of two tags’ initial phase offset (Sec. 2.2). To find out $\Delta\phi_{\text{Tag}}$, recall that the PDoA of two tags is bounded by $[\nu, \mu]$, where $\nu = -\frac{4\pi\hat{d}}{\lambda} + \Delta\phi_{\text{Tag}}$ and $\mu = \frac{4\pi\hat{d}}{\lambda} + \Delta\phi_{\text{Tag}}$ are the min and max PDoA values respectively, which are estimated by the ALS algorithm. Therefore, we can compute $\Delta\phi_{\text{Tag}}$ as follows:

$$\Delta\phi_{\text{Tag}} = \frac{\mu + \nu}{2}. \tag{9}$$

This offset is a constant value for a pair of tags, which will be subtracted from the measured PDoA value (modeled by Eq. (2)) before computing the orientation spectrum.

4.4 Dealing with the Blind Direction – Toward 3-DoF Orientation Tracking

The non-isotropic radiation of RFID tags limits the range of orientations that Tagyro can track using a single array. To realize 3-DoF orientation sensing, we propose a setup using dual-array and dual-antenna reader. As illustrated in Figure 15, our basic idea is to deploy another tag array along an orthogonal axis to the first one, so that it can compensate the blind direction, enabling full 2-DoF tracking. In addition, by deploying an additional reader antenna orthogonal to the first antenna, we can obtain total 4 DoFs (one being redundant). Compared to the 2-DoF case, 3-DoF orientation tracking requires an additional RFID antenna and tag array. Note that the dual-array can be attached not only to cuboid-shape objects, but also other arbitrary shapes (e.g., cylinder), as long as the two arrays can be arranged along perpendicular directions. We will present example use cases in Sec. 6.3.

Figure 15 illustrates Tagyro’s algorithmic modules under this new setup. During the initial setup, Tagyro needs to run the ALS algorithm for each tag array. At run time, it computes the orienta-

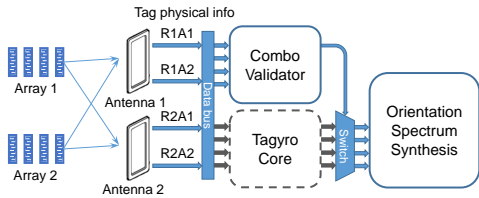


Figure 16: Processing blocks of the dual-array, dual-antenna reader setup for 3-DoF orientation sensing.

tion spectrum for each combination of tag array and reader-antenna, referred to as a *combo*. Meanwhile, it uses a *combo validator* to determine which combo evades the blind direction problem and provides a valid (low-noise) PDoA value. Each valid combo can track orientation along two axes. So, Tagyro runs an *orientation spectrum synthesis* scheme that unifies multiple valid combos' sensing results to generate a 3-DoF orientation.

4.4.1 Combo Validator

Recall that, when a tag's blind direction points near the reader antenna, the RSS of backscattered signals drops by more than 20 dB, and the phase values become erroneous (Sec. 4.2.2). In addition, to satisfy the polarity alignment constraint (Sec. 4.2.1), all tags within an array have the same blind direction. So, as the arrays rotate, Tagyro's combo validator tries to exclude those combos in which the array's blind direction points to the reader antenna. RSS may seem a potential indicator – a combo that measures low RSS is likely to experience the blind direction problem. However, the absolute RSS depends on the tag-to-antenna distance, which is a random unknown factor. Therefore, it is impractical to use a fixed RSS threshold for combo validation.

Our solution builds on the observation that, since the two arrays are in orthogonal directions, for each antenna, *at most one of the two arrays is in the blind direction*. Let Ω_1 and Ω_2 denote the average RSS for tags in Array 1 and 2 respectively. By comparing their average RSS, Tagyro can determine which array is in the blind direction:

$$\text{Blind_Direction_Array} = \begin{cases} 1, & \Omega_2 - \Omega_1 > \delta \\ 2, & \Omega_1 - \Omega_2 > \delta \\ \text{None}, & \text{otherwise} \end{cases}$$

i.e., when the RSS of one array is lower than the other by δ , it is considered to be blinded. Note that the threshold δ only depends on the relative RSS between a valid and blinded array, and is independent of the tag-to-antenna distance. Based on the empirical measurement in Figure 9, we set δ to a conservative value of 5 dB.

4.4.2 3D Orientation Spectrum Synthesis

In the dual-antenna reader setup, we take the first antenna's coordinate system as *primary*, and convert the estimation from the second antenna based on their geometrical relation. For example, in Figure 15, the orientation spectrum for the second antenna $I(\theta_Y, \theta_Z)$ in its own coordinate system becomes $I(\theta_X, \theta_Z)$ in the primary coordinate.

Tagyro merges the 2-DoF orientation spectrum (Eq. (3)) from different combos and produces a unified 3-DoF estimation. Let I_{RiAj} denote the 2-DoF spectrum of combo ij , comprised of Reader antenna i and Array j . Tagyro builds a new orientation spectrum in 3D space by summing the corresponding pixels across different combos. The synthesized spectrum for the setup in Figure 15 is:

$$I(\theta_X, \theta_Y, \theta_Z) = \sum_{j=1}^2 I_{R1Aj}(\theta_Y, \theta_Z) + \sum_{j=1}^2 I_{R2Aj}(\theta_X, \theta_Z).$$

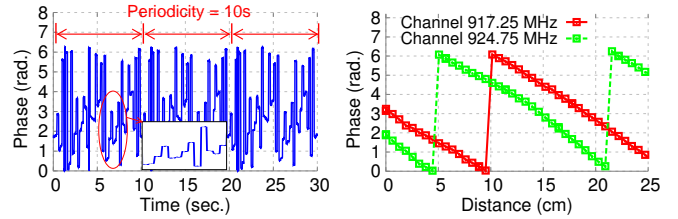


Figure 17: Phase jumping **Figure 18: Phase over distance for a fixed frequency.**

Similar to the 2-DoF case (Sec. 4.1), Tagyro finds the 3-DoF rotation angles by searching the maximum value in the 3D orientation spectrum.

4.5 Calibrating Frequency-Hopping Readers

To limit co-channel interference, commercial UHF RFID readers must randomly hop to one of 50 center frequencies within the 902-928 MHz band every 200 ms, following FCC regulation [27]. Frequency hopping will cause phase discontinuity due to the phase difference of oscillator and non-uniform frequency response of the tags' antennas. To our knowledge, this issue has not been examined experimentally in prior phase-based RFID sensing systems. So we first conduct an empirical study using the Impinj R420 reader [18].

We first measure the phase of a *stationary* tag, which shows huge phase discontinuity over 30 seconds (Figure 17). When zooming into a short period, we can see that phase values are piecewise constant with each piece lasting around 200 ms, corresponding the sojourn time on each frequency. On the other hand, Figure 18 shows that if we select the phase values from a single frequency and filter out others, the phase-distance relation still follows the linear model. These experiments imply that *different frequencies induce different initial phase-offsets at the reader*. To overcome the issue, one may selectively read the phase from one frequency, but this will significantly reduce the phase reading rate, because reader needs 10 seconds to finish one round of frequency hopping.

In Tagyro, we instead calibrate the phase difference between frequencies, so that the phase output looks like coming from a fixed frequency. The calibration is done by collecting an *initial phase measurement* that takes about 10s for an array before usage. Suppose during calibration, the tag is at distance d_0 to the reader, now the phase-distance relation in Eq. (1) also depends on frequency f_i , *i.e.*,

$$\phi(f_i, d_0) = \text{mod}\left(\frac{2\pi f_i d_0}{c} + \beta_i, 2\pi\right) \quad (10)$$

where c is light speed and β_i denotes the phase offset introduced at frequency f_i .

Given the initial phase measurement $\phi(f_i, d_0), \forall i \in [1, 50]$, we map the phase $\phi(f_i, d)$ for arbitrary distance d and frequency f_i to a common frequency f_r (default to 915.25 MHz). Substituting $\phi(f_i, d_0), \phi(f_r, d_0), \phi(f_i, d)$, and $\phi(f_r, d)$ into Eq. (10) and canceling the terms β_i and β_r , we have:

$$\phi(f_r, d) = \text{mod}\left([\phi(f_i, d) - \phi(f_i, d_0)] \frac{f_r}{f_i} + \phi(f_r, d_0), 2\pi\right). \quad (11)$$

Note that d and d_0 are not required to be known, because the phase value $\phi(f, d)$ is always read directly.

4.6 Dealing with Asynchronous Phase Reading

To compute the orientation of a tag array, the reader needs a synchronous phase snapshot of all tags. However, the EPC Gen2 RFID standard [17] adopts a Framed Slotted Aloha protocol which reads the tags asynchronously. To address this issue, Tagyro assumes the

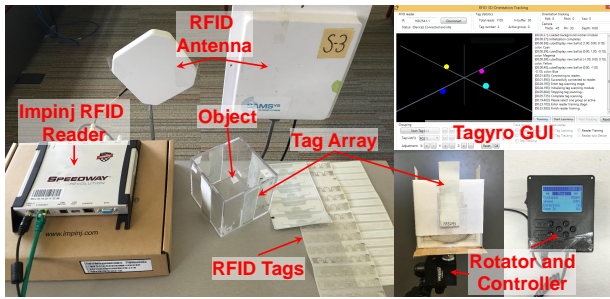


Figure 19: Tagyro implementation and software interface.

array’s rotation speed remains similar over consecutive phase readings (typically a few tens of ms), and uses an interpolation method, which creates an instant phase snapshot for all tags at an interval of every T phase readings. In Tagyro, we set T to the number of tags in array. Let $\phi(t_i)$ denote the phase of a tag at time t_i . Tagyro computes the snapshot phase at time stamp t , given historical phase readings at time t_i and t_{i-1} :

$$\phi(t) = \phi(t_{i-1}) + (\phi(t_i) - \phi(t_{i-1})) \frac{t - t_{i-1}}{t_i - t_{i-1}}. \quad (12)$$

Note out that since the interpolated phase value will be eventually updated by new phase measurement, the error of the interpolation result will not accumulate or propagate over time.

5. IMPLEMENTATION

Hardware: We implement a prototype of Tagyro using the COTS RFID reader Impinj R420 [18], which is FCC-compliant and performs frequency hopping within $902.75 \sim 927.25$ MHz. Figure 19 illustrates our hardware components. Two circular polarized antennas are connected to the reader via its two RF ports. Their antenna gain and 3 dB-beamwidth are 5.5 dBi, 7 dBi and 100° and 80° [28, 29], respectively. We assemble the tag array using three different types of RFID tags: ALN-9740 [30], SMARTRAC Dog-Bone [31], and SMARTRAC ShortDipole [32]. They are common label tag in flat, thin shape and commercially available [33]. Their maximum reading distance ranges from 15 ft to 20 ft. The reader interrogates RFID tags and sends query reports, containing information of ID, RSS, phase, time stamp and channel, via Ethernet to a host PC that runs Tagyro.

Software: Tagyro’s software implementation contains three major modules: 3D GUI, RFID library and processing algorithms. The GUI module is developed in C#. It displays the tag array’s effective layout during initial setup, and instantaneous orientation during run-time tracking. The RFID library controls the reader using a Low-Level Reader Protocol (LLRP) ratified by EPCglobal. We implement Tagyro’s key processing algorithms (Sec. 4) in MATLAB, and then recompile them into standalone C libraries (DLL) using the Code Generation toolbox. The C libraries are imported into C# program and being invoked in real-time. To start, we first run the frequency calibration module for each array. Then we randomly rotate the tag array when Tagyro performs ALS to sense the tag array’s effective layout. Afterwards, Tagyro can begin its orientation tracking.

6. EVALUATION

Methodology: We conduct experiments in an office environment to evaluate the effectiveness of Tagyro’s design components, accuracy of orientation sensing, as well as run-time latency. Figure 15 illustrates our experiments’ default setup, where 4 DogBone tags are attached to a plastic cube forming a square tag array, separated

roughly by quarter-wavelength (*i.e.*, 8.2 cm). Note that since our ALS algorithm can automatically sense the tag layout, it is not required to deploy the RFID tags with precise separation. Two reader antennas are placed 1 m away from the tag array at mutually perpendicular directions, both 70 cm above the ground. By default, the reader uses its maximum transmit power at 32 dBm.

Since we are unaware of any RFID-based system that tracks 3D orientation of an object, we evaluate accuracy of Tagyro against ground truth measurement. To obtain the ground-truth orientation, we mount the tag array (attached to an object) on a mechanical rotator [34] (Figure 19), which is controlled by the PC host to rotate at full 360-degree at maximum speed 1.71 rad/s with minimum granularity of 1° . We first rotate the tag array to a known orientation, and use it as the initial state. Then, the offset between the motor’s rotation angles and initial state is used as the ground-truth orientation. Since the motor can only rotate in one DoF, we manually change the pose of the tag array, so that different DoFs can be aligned to the motor’s rotation axis.

Metrics: To characterize Tagyro’s accuracy, we mainly focus on angular error, *i.e.*, the deviation of estimated orientation angle from the ground truth. Since Tagyro mainly relies on the PDOA information to pinpoint the tag orientation, in the micro-benchmark experiments we also use the phase error to quantify the effectiveness of our design.

6.1 Micro Benchmarks

Effectiveness of sensing effective layout. Recall a tag array’s effective layout sensed by ALS may differ from the physical geometry, due to tag coupling. Figure 20 illustrates the layout of a 4-tag square array for cases with and without the coupling effect. Note that in the effective layout, two tags deviate from the Z axis in order to virtually compensate the coupling effect. Yet, obtaining the ground truth of coupling effect requires the knowledge of tag’s physical parameters, *e.g.* coupling coefficient, which are not easily accessible in practice. On the other hand, the ALS accuracy will directly affect the ultimate performance of orientation tracking. Thus, we leave the evaluation of its effectiveness in the system level tests (Sec. 6.2).

To validate whether ALS can indeed counteract the coupling effect, we compute the orientation spectrum with effective layout. For contrast, we also simulate the oracle case using physical layout in a non-coupling scenario, which produces the ideal orientation spectrum. Generally, higher peak intensity means better spectrum (with higher contrast), because tracking will be more resilient to noise and spatial ambiguity. Figure 21 plots a snapshot spectrum in one dimension for θ_z by fixing θ_x and θ_y to zero. When the array is orientated at $(0, 0, 195^\circ)$, the orientation spectrum from ALS has similar peak intensity as oracle. Compared with the case when the physical layout is used directly, ALS significantly improves the contrast of spectrum. Figure 22 statistically plots the difference of highest intensity peak in spectrum relative to the oracle. The ALS algorithm reduces the intensity difference by $5.5\times$ compared with using physical layout.

Accuracy of selecting the valid combo. In 3D orientation tracking, Tagyro’s combo validator is critical in dealing with the blind direction issue. We verify this mechanism by rotating two arrays together in 3D space, and inspect if Tagyro can select the correct tag array. We determine the ground truth by checking if an array’s blind direction is within 40° pointing to the reader antenna.

The experiment results in Figure 23 show that the array indices selected by Tagyro all match the ground truth. Since occasional blockage can also cause RSS offset between the two arrays to exceed the conservative threshold $\delta = 5dB$ (Sec. 4.4), some array

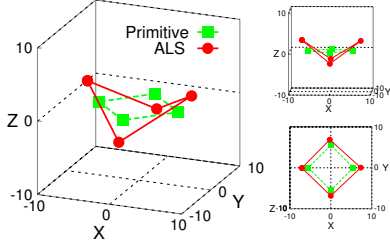


Figure 20: Effective and physical layout of the 4-tag array.

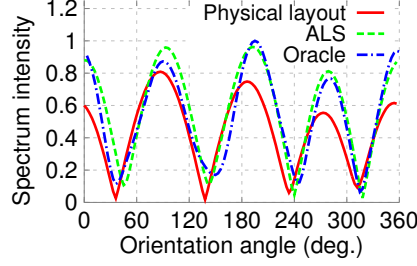


Figure 21: Normalized Spectrum for 4-tag array.

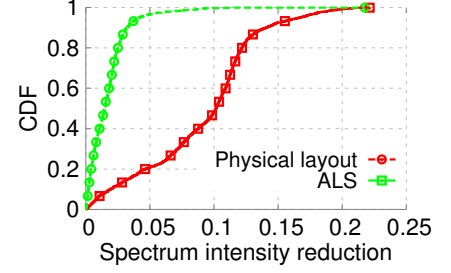


Figure 22: The CDF of spectrum intensity difference compared to the oracle.

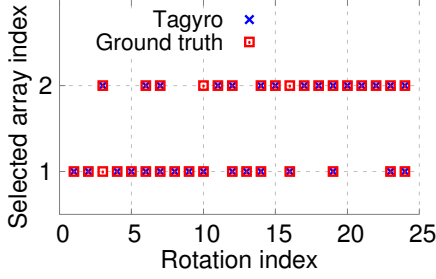


Figure 23: Accuracy of selecting the array in the valid reading zone.

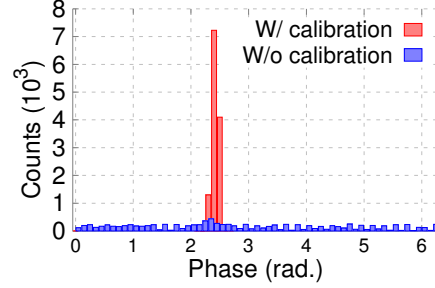


Figure 24: Histogram of phase distribution for frequency hopping calibration.

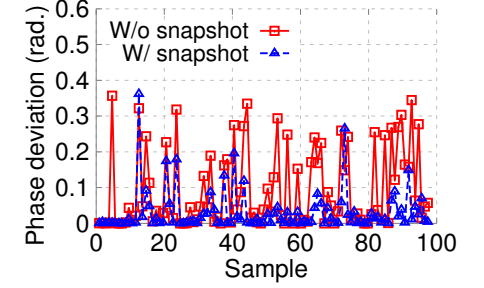


Figure 25: Residual phase error of asynchronous phase reading.

Table 1: Query frequency of each tag in the array (SPS).

Tag #	4	6	8
Avg. spd.	43.1	40.0	37.7
10% spd.	32.1	26.8	25.1
90% spd.	50.0	47.9	46.6

Table 2: Efficiency of the tracking algorithm (FPS).

Tag #	4	6	8
1-DoF	4618	3653	3423
2-DoF	205	145	121
3-DoF	111	77	63

indices in the ground truth may not be identified by Tagyro. However, this will not cause error because Tagyro can still use the other array to compute the orientation.

Channel hopping calibration. We next evaluate the impact of reader’s channel hopping on the phase value by measuring the phase of a *static* tag for 2 minutes. Figure 24 plots the histogram of phase values. Without calibration, phases are almost evenly distributed over all possible values with a *std.* of 1.78-radian. However, the *std.* is reduced by 46 \times , down to 0.039-radian after applying the calibration, which is very close to the noise floor 0.025-radian.

Effectiveness of the phase snapshot algorithm. Tags in an array are queried asynchronously by the reader, which makes the timestamps of phase reading misaligned. To evaluate this impact, we first rotate the tag array over 100 preset orientations and measure the phase values. Since the tag array is stationary during each measurement, the phase readings are consistent and used as ground-truth. Then we measure the phase while continuously rotating the array through these preset orientations. We observe that the phase error is substantially reduced after applying the phase snapshot algorithm (Figure 25). Mean error drops from 0.084 radian to 0.026 radian. We believe the reduction can be larger for a higher rotation speed. Note that the error can occasionally be magnified by the phase snapshot due to unexpected phase deviation, *e.g.* noise. But they will have marginal impact on orientation tracking since the occasionally magnified error does not accumulate or propagate over time.

Interrogating speed of tag array. For real-time orientation tracking, one key question is: how fast can the RFID reader query the

tag array? The query speed determines how frequent Tagyro can update the orientation estimation. We evaluate the query speed by interrogating different sizes of tag arrays. The reader uses its default *AutoSet Dense* mode, which automatically adjusts its MAC-layer parameters to maximize the tag query speed. Table 1 summarizes the CDF of update frequency for a two-minute measurement when the array rotates at the maximum speed. Although the update frequency slightly decreases as we increase the array size, on average Tagyro can achieve 37.7 samples per second (SPS) even for the 8-tag array.

Efficiency of tracking algorithm. We further examine the real-time processing speed of our Tagyro implementation. We first collect a 2-minute trace data of the tag array’s phase and then replay the trace in our Tagyro program. In this way, we can evaluate the efficiency of our orientation tracking algorithm independently of the reader’s query speed. We run Tagyro on a i7-4770 PC utilizing one CPU core. Table 2 plots the frame rate (number of orientation sample outputs per second). Tagyro can maintain an average processing rate of 3500 FPS, 144.8 FPS and 76.7 FPS, for 1-DoF, 2-DoF and 3-DoF orientation tracking, respectively. The main bottleneck of Tagyro’s tracking efficiency lies in the RFID reader’s query speed (Table 1) which is much lower than the processing speed of Tagyro.

6.2 System Level Tests

We proceed to evaluate Tagyro’s overall performance in tracking 3D orientation under various practical settings.

Accuracy of 3D orientation tracking. We first evaluate the accuracy of orientation tracking under different DoFs: (i) *1-DoF*: tracking Z-axis rotation using a single tag array and single-antenna reader; (ii) *2-DoF*: tracking Y and Z axis rotations using dual-array and single-antenna reader; (iii) *3-DoF*: using the dual-array, dual-antenna reader setup as in Figure 15. Our experimental results (Figure 26) show that for both 1-DoF and 2-DoF, the average (90-percentile) tracking error is about 4 $^{\circ}$ (8 $^{\circ}$). 2-DoF case has a similar accuracy with the 1-DoF since each of the two arrays independently

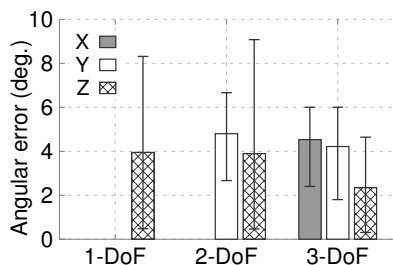


Figure 26: Accuracy vs. DoF. Error bar shows the 90th error.

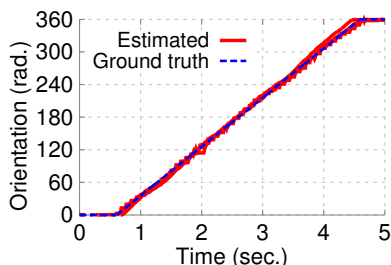


Figure 27: Estimation and ground-true for 1-DoF rotation.

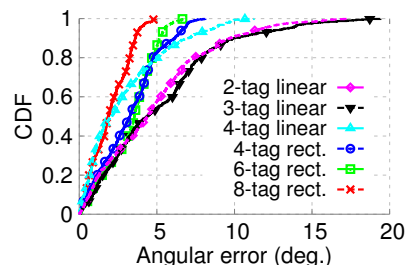


Figure 28: The CDF of orientation error vs. size of tag array.

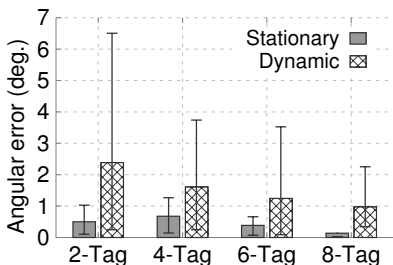


Figure 29: Orientation error under surrounding human activity. Error bar shows the 90th error.

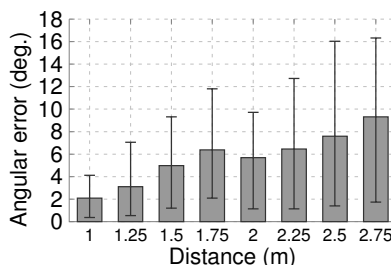


Figure 30: Orientation error over tag-to-antenna distance.

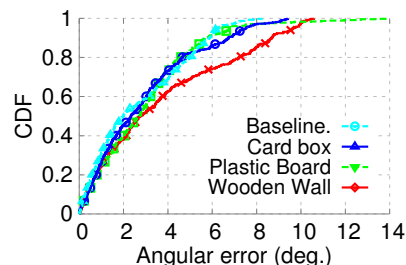


Figure 31: The CDF of orientation error under blockage.

tracks one DoF. Notably, the average orientation error of Z-axis is much smaller (2.2°) in 3-DoF case, because both of the reader’s antennas are outside the blind direction. Tagyro’s orientation spectrum synthesis can effectively unify the extra spatial diversity to produce a better estimate. Figure 27 plots 5 overlapped example tracking results for 360° rotation in 1-DoF. The figure depicts the orientation estimation of a tag array rotating at a constant speed and the ground truth value over the time, which shows that the estimated angle is highly consistent with the ground truth at every time stamp.

Impact of array size. We next vary the number of tags in array from 2 to 8 and evaluate how it affects the accuracy of orientation tracking. Figure 2 shows the tag arrays’ physical layouts. Figure 28 plots the CDF of angular error in 1-DoF tracking, which shows that *a larger tag array can effectively improve accuracy*. The average error is reduced from 4.80° for 2-tag array to 1.98° for 8-tag array. Moreover, the 90-percentile error is also reduced from 9.71° to 3.60° . The improvement gently diminishes as the size of tag array increases. In practice, an array of 4~6 tags may make a good balance between accuracy vs. form factor. Using high-frequency tags (*e.g.*, millimeter-wave) may significantly reduce the form factor due to shorter wave length and smaller antenna size. But this is beyond the scope of our work.

Impact of environmental dynamics. Like all other phase-based RFID sensing systems [8–10, 13], estimated phase value in Tagyro is subject to the channel noise and influenced by multipath environment. To evaluate their impacts, we measure the jitter of estimated orientation, while fixing the tags so that any jitter can be only caused by RF channel fluctuation. Figure 29 compares the angular jitter in a stationary environment with that where a human randomly walks around the reader and tags. The average jitter caused by the channel noise itself is small and typically less than 1° . On the other hand, the estimated orientation can deviate by 6.5° when there is significant human movement. This is mainly attributed to the intentionally created variation of multipath reflections. Fortunately, a larger tag array can make Tagyro more resilient to environmental dynamics — with an 8-tag array, the angular jitter is reduced to about 1° .

Impact of tag-to-antenna distance. Typical RFID systems have a maximum reading range of 4~6 m [35]. Longer distance results in weaker signals, hence more noisy phase reading. To understand its impact on the orientation accuracy, we vary the tag-to-antenna distance from 1 m to 2.75 m. Figure 30 shows that the average angular error gently increases from 2.09° to 9.32° , with a maximum working distance about 3m in our setup. A closer examination reveals that the RSS drops significantly over distance. The lowest RSS across rotation angles decreases by more than 21 dBm, from -49 dBm at 1m to -70 dBm at 2 m. Since the sensitivity of the Impinj R420 reader is -82 dBm [18], its measured phase value starts to deviate from the phase-distance model (Sec. 2.1) when distance goes beyond 2 m. On the other hand, backscattered data bits can be decoded at a further distance because RFID adopts Amplitude-Shift Keying (ASK) modulation that is insensitive to the phase deviation. By deploying more RFID antennas, Tagyro can potentially cover a wider working area, which we will leave for our future work.

Under blockage. Tagyro’s usage scenarios may involve NLOS environment, *e.g.*, in a supply chain, where the object (and tag array) may be placed inside a card box (Figure 1). We mimic such NLOS cases by blocking the LOS between the tag array and reader using different materials: card box, plastic board and wooden wall, with thickness of 5 mm, 10 mm and 30 mm, respectively. Figure 31 shows that blockage has marginal impact on Tagyro’s orientation tracking. The wooden wall slightly reduces the accuracy because its thickness attenuates the backscattered signal strength, similarly to increasing tag-to-reader distance. The experiment verifies that Tagyro can track orientation in NLOS scenarios where camera-based approaches [36] will fail.

Latency of rotation response. In the implementation, we buffer multiple latest phase values for algorithm processing and adopt a Kalman filter to reduce noise in orientation estimation. They will incur response latency in the tracking output. To evaluate the latency, we rotate the tag array by 90° and simultaneously measure the time it takes for the estimated orientation to be less than 5° close to the ground truth. Figure 32 plots the CDF of response latency from 50 measurements. The average values of response latency are

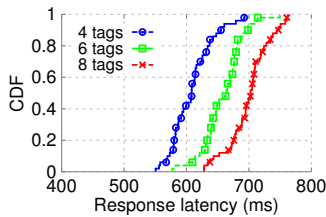


Figure 32: Latency of rotation response.

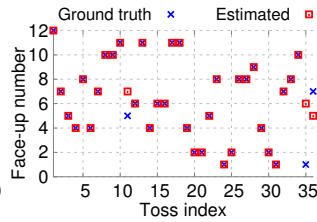


Figure 33: Detecting which side of the dice faces up.

0.61s and 0.71s for 4-tag and 6-tag arrays respectively, which are sufficient for most application scenarios that do not have stringent timing constraint. Besides, the latency can be further reduced by using high-speed RFID readers.

6.3 Case Study

In this section, we apply Tagyro in two case studies: a gaming scenario where Tagyro detects the orientation of a 12-side dice, and a smart home scenario where Tagyro monitors the rotation of the door and consumption of roll tissue.

Tracking a 12-side dice. To detect which side of a ball-like dice faces up, we need at least two DoFs – the horizontal rotation does not matter because it will not change the face-up number. Thus, we setup one reader in the ceiling, which projects signals toward the ground and attach two tag arrays to the dice in mutually perpendicular directions (Figure 34). We randomly toss the dice and record the estimated and ground-truth number that faces up. Figure 33 shows that Tagyro correctly identifies 33 out of 36 numbers, achieving 91.7% accuracy. The tracking accuracy of the 12-side dice is lower than the 3D case (Figure 26) due to two factors. *First*, the shape of dodecahedron does not allow us to attach tags completely following the constraint of polarity alignment (Section 4.2.1), which reduces the accuracy of combo validation (Section 4.4.1). *Second*, the two closely-placed tag arrays will create an inter-array coupling effect. Tagyro performs ALS independently for each array, which handles the intra-array coupling effect. Yet, it is unable to sense the inter-array coupling effect. On the other hand, Tagyro cannot perform a joint ALS for both arrays because their polarity directions are orthogonal. One approach to mitigate the inter-array coupling effect is to separate the two arrays by a distance of greater than half-wavelength (Figure 12), such as attaching tags to different edges of the box (Figure 15).

Monitoring smart home. In the smart home scenario, Tagyro can monitor the status of daily objects, *e.g.*, whether the door is open or close, which direction a rolling chair (and a seated human) is facing, and how much roll tissue has been consumed. Many such problems can be addressed by sensing the rotation/orientation of the passive objects. Here we showcase the door and roll tissue scenarios. Since both of them have fixed rotation axes, (*i.e.*, rotation is restricted to 1-DoF), we attach a 4-tag array on each (Figure 1), and use a single-antenna reader as monitor. Figure 35(a) plots the accumulated rounds of rotations for a roll tissue, which unveils fine-grained information of the consumption over time. Figure 35(b) shows tracking result for a door, which measures not only its opening angle, but also the time duration when it stays open/close. These case studies also demonstrate Tagyro can be applied to a wide range of objects with different shapes.

Though these detection tasks may be also addressed by simple mechanical or IR sensor, Tagyro has several unique advantages over them. (*i*) Fine-grained rotation trajectory. Tagyro not only tells if the door opens or closes, but also the degree of opening, which is useful for applications, such as to determine if a robot or cargo can



Figure 34: Eight tags are attached to the surface of a 12-side dice.

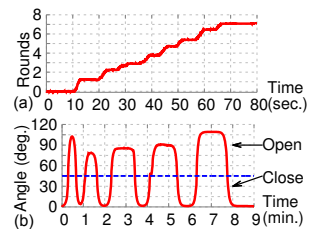


Figure 35: Detecting (a) usage of roll tissue and (b) open/close status of the door.

go through the door. (*ii*) Ad-hoc installation. Tagyro can instantly enable orientation tracking by attaching multiple tags to the target object, which does not involve heavy mechanical installation or altering the physical structure. (*iii*) Maintenance free. The batteryless RFID tags are continuously powered by the RFID reader without the need for battery replacement.

7. DISCUSSION

Multipath Effects: Besides RFID tags, signals from the RFID reader may be reflected by other objects in the environment. Reflections from stationary objects do not disturb the RFID phase measurement [13], and hence will not affect Tagyro’s performance. RFID reader estimates phase based on the modulated signals back-scattered from the tag. Any signals reflected from static objects are unmodulated and are already removed by the reader’s built-in high-pass filter.

Yet, multipath reflections from moving objects, *e.g.*, human walking, may cause some adversary effects. In such cases, the reflected signals are dynamic, and thus may not be effectively removed by the high-pass filter. Fortunately, this adversary impact can be effectively alleviated by increasing the tag number in the array (Figure 29).

Coupling Effect Caused by Surrounding Metallic Objects: The coupling effect occurs not only among RFID tags, but also between the tag and surrounding metallic materials in the environment, which we call *static* and *dynamic* coupling, respectively. The ALS algorithm is designed primarily to address the static coupling issue. The dynamic coupling cannot be effectively captured, because the metallic object does not rotate along with the tag array – when the tag array rotates, their coupling coefficients would change arbitrarily. Addressing the impact of dynamic coupling effect from surrounding metallic objects on the RFID phase measurement is still an open challenge. Fortunately, our observation (Figure 12) demonstrates that as long as the metallic object is not very close to the tag, *e.g.*, $>$ the half wavelength ($\frac{\lambda}{2} \approx 16cm$), the coupling effect between them will almost vanish and will not affect the accuracy of phase measurement.

Size of Tag Array: Given the relatively large size of commodity UHF RFID tags, it may not always be feasible to attach multiple tags to an object of small size. The size of tag array is primarily limited by the physical constraint, where the antenna size and separation have to match the wavelength of wireless frequency. As the RFID technology matures at higher frequency, *e.g.*, 60 GHz, the size of tag array can be significantly reduced [37, 38], much like a finger nail. A smaller tag size will extend Tagyro towards more ubiquitous Internet-of-Things applications.

Tracking Orientation of Multiple Objects: When multiple objects exist in the same vicinity, Tagyro can track them independently given the tag IDs associated with each object. This is a huge advantage over vision-based approaches [3–7] which are eas-

ily confused by background and occlusion effects. Yet, the performance of Tagyro may be compromised due to the limited total query speed of the RFID reader, where the speed for each tag is reduced.

8. RELATED WORK

Our work is most closely related with prior art in the following domains:

Sensor-equipped device. The most straightforward approach to sense orientation is to use active sensors, *e.g.*, magnetometer, gyroscope or accelerometer. Acube [15] combines these active sensors to estimate the orientation of a smartphone that is used for indoor localization and tracking. In industry setting [39], orientation sensors are deployed to guide robot arms to pick up objects. Active sensors are accurate but power hungry, and need frequent maintenance (*e.g.*, battery replacement or charging). RFID tags are batteryless and ideal for objects that cannot afford frequent maintenance. RFID-Die [40] and WISP [41] use customized RFID tags with embedded motion sensors that harvest energy from RF signals. The power draw of sensors significantly reduces the tags' working range (down to 8 cm [40]) and reduces the duty cycle (*e.g.*, one sensing for every two-second charging [42]). In contrast, Tagyro uses COTS passive RFID tags, with a typical working range of around 3 m and sampling rate of 37.7 samples/second. Owing to low-cost of RFID tags (10 cents each [43]), Tagyro is readily usable in massive Internet-of-Things applications. In addition, mid-end smartphones with RFID readers are already available, which can bring Tagyro to home and in-situ usage. The Cricket Compass [44] tracks the orientation of a mobile device based on the distance difference of arrival between multiple pairs of ultrasonic transceivers. Although the high-level principle share similarities, Tagyro's RFID tag array tracking entails a unique set of challenges while bringing salient properties in terms of precision, cost, and energy efficiency.

Image-based orientation detection. Detecting the orientation of object is a general problem in computer vision [3–7]. Hinterstoisser *et al.* [3] proposed a template matching method to detect the tilt angle of objects in the image. Image-based approach is also used to detect human face, head and gaze orientation [45, 46]. Saxena *et al.* [4, 36] and Shimizu *et al.* [7] applied a pattern matching method to estimate the 3D orientation of objects in the image, which can guide robotic arms' grasping action. However, such image-based approaches only work in line-of-sight (LOS). They are very sensitive to lighting condition and fail even under partial occlusion by a paper box. On the other hand, Tagyro can accurately track object orientation even if the tags are occluded from the reader's LOS.

RFID tilt sensing. There has been preliminary work in RFID-based tilt sensing, which puts either the reader or tags on the object. Han *et al.* [47, 48] used a site-survey approach to determine the position and orientation of a target (*e.g.* robot and chair) in a 2D space. However, they need to install the reader on the target, and require a dense deployment of RFID tags to cover the floor of interest. RF-Compass [12] uses a 2D-plane partitioning method to navigate a robot to gradually converge towards an object's direction, but cannot estimate the object's instantaneous 3D orientation. Krigslund *et al.* [14, 49, 50] estimate the 1D orientation of an RFID tag by tracking the RSS fluctuation based on the principle of antenna polarity. Due to polarity mismatch, RSS decreases proportionally to the angular misalignment between the reader and the tag. However, the RSS is easily affected by distance and environment dynamics, and the polarity-based approach has 90° ambiguity in orientation estimation. Tagyro represents the first phase-based method to sense tag orientation without ambiguities, and in 3D space.

RF-based localization. RFID tag localization has been exten-

sively studied recently [8, 10, 47, 48, 51, 52]. The state-of-the-art techniques, *e.g.*, Tagoram [8] and PinIt [52], can already locate the tag's position at a cm-level or mm-level accuracy. On the other hand, estimating the orientation of RFID tag is a relatively new area that has not been well explored yet. The basic idea behind Tagyro's tag array approach shares similar spirit with antenna-array based radio localization [53], which can track the relative angle between a multi-antenna receiver and an access point on the same 2D space. However, the unique properties of RFID, *e.g.*, tag coupling and non-isotropic radiation, bring unprecedented challenges to Tagyro.

One may think of applying them to estimate the object orientation: by attaching two tags to different parts of the object, its orientation can be derived from the estimated locations of tags. However, this approach has several limitations. *First*, existing schemes only address the 2D localization problem [47, 48, 51]. The 2D position (on a plane) limits the orientation estimation to only 1 DoF. *Second*, most state-of-the-art localization schemes have 10~20 cm errors [10]. They are unable to differentiate the position of two closely-placed tags, and thus cannot give precise orientation estimation. Although Tagoram [8] can estimate tag position at cm-level accuracy, it requires multiple readers that are precisely deployed at dedicated positions, which is not suitable for ad-hoc scenarios like smart home or mobile gaming. STPP [11] can estimate the relative position for closely-separated tags, but it can only discriminate the left/right/up/down ordering. Furthermore, the non-ideal radiation of RFID signal (Sec. 4.2) invalidates the basic assumption that the phase changes linearly over distance, which requires us to re-think the effectiveness of existing phase-based RFID localization techniques [8, 11] when working in the 3D space.

RFID radiation pattern. Existing electromagnetic research has studied the imperfection of RFID tag radiation pattern. Zhang *et al.* [54] used two dipole antennas in orthogonal directions to achieve full RSS coverage over 3D space. Tagyro adopts a similar idea to address the blind direction issue, which deploys two tag arrays in perpendicular directions (Sec. 4.2). Yet, Tagyro addresses the more critical problem of polarity-induced phase-shifting, through adaptive array selection and polarity alignment. Bolotnyy *et al.* [55] studied the tag readability issue caused by coupling effect in a multi-tag RFID system. To our knowledge, Tagyro is the first to evaluate the impact of coupling effect on the phase of RFID tag array, and to counteract the effect by using the layout sensing technique.

9. CONCLUSION

In this paper, we propose an RFID-based system to track the orientation of a batteryless object. By forming an array using multiple tags, Tagyro exploits their phase difference of arrival to find out the object orientation. Novel processing algorithms are proposed to address challenging issues such as coupling effect, which are raised in the tag-array RFID system. Tagyro is built upon COTS RFID reader and tags. We conduct system-level experiments and two case studies, which show that Tagyro can achieve high accuracy in orientation tracking. Tagyro represents the first study of an RFID-based 3D orientation tracking system, which can be applied to many practical scenarios including but not limit to smart home and mobile gaming.

Acknowledgements

We appreciate the insightful feedback from the anonymous reviewers who helped improving this work. This project is supported in part by the NSF under Grant CNS-1506657, CNS-1518728, CNS-1343363, and CNS-1350039.

10. REFERENCES

- [1] H. Wang, M. Farid, S. Sen, M. Youssef, A. Elgohary, and R. R. Choudhury, "No Need to War-drive: Unsupervised Indoor Localization," in *Proceedings of ACM MobiSys*, 2012.
- [2] S. Agrawal, I. Constandache, S. Gaonkar, R. Roy Choudhury, K. Caves, and F. DeRuyter, "Using Mobile Phones to Write in Air," in *Proc. of ACM MobiSys*, 2011.
- [3] S. Hinterstoisser, V. Lepetit, S. Ilic, P. Fua, and N. Navab, "Dominant Orientation Templates for Real-Time Detection of Texture-less Objects," 2010.
- [4] A. Saxena, J. Driemeyer, and A. Y. Ng, "Learning 3-D Object Orientation From Images," in *Robotics and Automation, 2009. ICRA'09. IEEE International Conference on*, 2009.
- [5] A. Collet, D. Berenson, S. S. Srinivasa, and D. Ferguson, "Object Recognition and Full Pose Registration from a Single Image for Robotic Manipulation," in *IEEE International Conference on Robotics and Automation (ICRA)*, 2009.
- [6] W. Wan, F. Lu, Z. Wu, and K. Harada, "Teaching Robots to Do Object Assembly Using Multi-Modal 3D Vision," *arXiv preprint arXiv:1601.06473*, 2016.
- [7] S. Shimizu, T. Nagahashi, and H. Fujiyoshi, "Robust and Accurate Detection of Object Orientation and ID Without Color Segmentation," in *RoboCup 2005: Robot Soccer World Cup IX*, 2005.
- [8] L. Yang, Y. Chen, X.-Y. Li, C. Xiao, M. Li, and Y. Liu, "Tagoram: Real-Time Tracking of Mobile RFID Tags to High Precision Using COTS Devices," in *ACM MobiCom*, 2014.
- [9] T. Liu, L. Yang, Q. Lin, Y. Guo, and Y. Liu, "Anchor-Free Backscatter Positioning for RFID Tags With High Accuracy," in *Proc. of IEEE INFOCOM*, 2014.
- [10] J. Wang, D. Vasisht, and D. Katabi, "Rf-iDraw: Virtual Touch Screen in the Air Using RF Signals," in *ACM SIGCOMM Computer Communication Review*, 2014.
- [11] L. Shangquan, Z. Yang, A. X. Liu, Z. Zhou, and Y. Liu, "Relative Localization of RFID Tags Using Spatial-Temporal Phase Profiling," in *Proc. of USENIX NSDI*, 2015.
- [12] J. Wang, F. Adib, R. Knepper, D. Katabi, and D. Rus, "RF-Compass: Robot Object Manipulation Using RFIDs," in *Proc. of ACM MobiCom*, 2013.
- [13] P. V. Nikitin, R. Martinez, S. Ramamurthy, H. Leland, G. Spiess, and K. Rao, "Phase Based Spatial Identification of UHF RFID Tags," in *RFID, 2010 IEEE International Conference on*, 2010.
- [14] R. Krigslund, P. Popovski, G. F. Pedersen, and K. Bank, "Potential of RFID Systems to Detect Object Orientation," in *IEEE International Conference on Communications (ICC)*, 2011.
- [15] P. Zhou, M. Li, and G. Shen, "Use It Free: Instantly Knowing Your Phone Attitude," in *Proc. of ACM MobiCom*, 2014.
- [16] "Low Level User Data Support," *Speedway Revolution Reader Application Note*, 2013.
- [17] M. Roberti, "EPCglobal Ratifies Gen 2 Standard," *RFID Journal*, 2004.
- [18] "Impinj RFID Reader." [Online]. Available: <http://www.impinj.com/products/readers/>
- [19] L. Shangquan, Z. Yang, L. Alex, and Y. Liu, "Relative Localization of RFID Tags Using Spatial-Temporal Phase Profiling," in *USENIX NSDI*, 2015.
- [20] T. Liu, L. Yang, Q. Lin, Y. Guo, and Y. Liu, "Anchor-Free Backscatter Positioning for RFID Tags With High Accuracy," in *Proc. of IEEE INFOCOM*, 2014.
- [21] H. Lehpamer, *RFID Design Principles*. Artech House, 2012.
- [22] H. S. Lui, "Mutual Coupling in Antenna Arrays," 2010.
- [23] H. Hui and S. Lu, "Receiving Mutual Impedance between Two Parallel Dipole Antennas," in *Proceedings of the IEEE TENCON*, 2006.
- [24] K. Abbas, "A New Recurrent Approach for Phase Unwrapping," *International Journal of Applied Science and Engineering*, 2005.
- [25] I. Borg and P. J. Groenen, *Modern Multidimensional Scaling: Theory and Applications*. Springer Science & Business Media, 2005.
- [26] T. Yang, J. Liu, L. McMillan, and W. Wang, "A Fast Approximation to Multidimensional Scaling," in *IEEE workshop on Computation Intensive Methods for Computer Vision*, 2006.
- [27] M. Buettner and D. Wetherall, "A Gen 2 RFID Monitor Based on the USRP," *ACM SIGCOMM Computer Communication Review*, 2010.
- [28] "Patch Antenna (Circular) A0003-02," <http://www.atlasrfidstore.com/inven-go-xc-1003-uhf-rfid-mobile-phone>, 2015.
- [29] "Mini RFID Panel Antenna S9025P," <http://www.es.co.th/Schemetic/PDF/S9025PR-S9025PL.PDF>, 2009.
- [30] "ALN-9740 Squiggle Inlay," <http://www.alientechnology.com/wp-content/uploads/Alien-Technology-Higgs-4-ALN-9740-Squiggle.pdf>.
- [31] "Dogbone - Smartrac," https://www.smartrac-group.com/files/content/Products_Services/PDF/DogBone_M4.pdf.
- [32] "ShortDipole - Smartrac," https://www.smartrac-group.com/files/content/Products_Services/PDF/ShortDipole_M5.pdf.
- [33] "RFID Tag Type Options," http://www.idtechex.com/research/articles/rfid_tag_type_options_00000041.asp.
- [34] "Axis360 Motion Control System," <http://cinetics.com/two-axis360/>.
- [35] R. Want, "An Introduction to RFID Technology," *Pervasive Computing, IEEE*, 2006.
- [36] A. Saxena, J. Driemeyer, and A. Y. Ng, "Robotic Grasping of Novel Objects Using Vision," *The International Journal of Robotics Research*, 2008.
- [37] S. Pellerano, J. Alvarado, and Y. Palaskas, "A mm-wave power-harvesting rfid tag in 90 nm cmos," *IEEE Journal of Solid-State Circuits*, 2010.
- [38] P. Pursula, T. Karttaavi, M. Kantanen, A. Lamminen, J. Holmberg, M. Lahdes, I. Marttila, M. Lahti, A. Luukanen, and T. Vaha-Heikkilä, "60-ghz millimeter-wave identification reader on 90-nm cmos and ltcc," *IEEE Transactions on Microwave Theory and Techniques*, 2011.
- [39] G. Fortino and P. Trunfio, "Internet of Things Based on Smart Objects," *Fortino & P. Trunfio, eds., Cham: Springer International Publishing*, 2014.
- [40] L. Büthe, M. Hardegger, P. Brülisauer, and G. Tröster, "RFID-Die: Battery-Free Orientation Sensing Using an Array of Passive Tilt Switches," in *Proceedings of ACM*

International Joint Conference on Pervasive and Ubiquitous Computing: Adjunct Publication, 2014.

- [41] D. J. Yeager, A. P. Sample, J. R. Smith, and J. R. Smith, "Wisp: A Passively Powered UHF RFID Tag With Sensing and Computation," *RFID Handbook: Applications, Technology, Security, and Privacy*, 2008.
- [42] J. R. Smith, A. P. Sample, P. S. Powledge, S. Roy, and A. Mamishev, "A Wirelessly-Powered Platform for Sensing and Computation," in *ACM UbiComp*, 2006.
- [43] X. Zhu, S. K. Mukhopadhyay, and H. Kurata, "A Review of RFID Technology and Its Managerial Applications in Different Industries," *Journal of Engineering and Technology Management*, 2012.
- [44] N. B. Priyantha, A. K. Miu, H. Balakrishnan, and S. Teller, "The Cricket Compass for Context-Aware Mobile Applications," in *Proc. of ACM MobiCom*, 2001.
- [45] C.-C. Chang and H. Aghajan, "Collaborative Face Orientation Detection in Wireless Image Sensor Networks," in *Proceedings of ACM SenSys Workshop on Distributed Smart Cameras*, 2006.
- [46] J. Y. Kaminski, J. Teicher, and A. Shavit, "Head Orientation and Gaze Detection from a Single Image," in *International conference of computer vision theory and applications*, 2006.
- [47] S. Han, H. Lim, and J. Lee, "An Efficient Localization Scheme for a Differential-Driving Mobile Robot Based on RFID System," *Industrial Electronics, IEEE Transactions on*, 2007.
- [48] A. A. N. Shirehjini, A. Yassine, and S. Shirmohammadi, "An RFID-Based Position and Orientation Measurement System for Mobile Objects in Intelligent Environments," *Instrumentation and Measurement, IEEE Transactions on*, 2012.
- [49] R. Krigslund, S. Dosen, P. Popovski, J. L. Dideriksen, G. F. Pedersen, and D. Farina, "A novel technology for motion capture using passive uhf rfid tags," *IEEE Transactions on Biomedical Engineering*, 2013.
- [50] G. Gupta, B. P. Singh, A. Bal, D. Kedia, and A. Harish, "Orientation detection using passive uhf rfid technology [education column]," *IEEE Antennas and Propagation Magazine*, 2014.
- [51] S. Hinske, "Determining the Position and Orientation of Multi-Tagged Objects Using RFID Technology," in *IEEE Pervasive Computing and Communications Workshops*, 2007.
- [52] J. Wang and D. Katabi, "Dude, where's my card?: RFID Positioning That Works With Multipath and Non-Line of Sight," *ACM SIGCOMM Computer Communication Review*, 2013.
- [53] J. Xiong and K. Jamieson, "ArrayTrack: A Fine-Grained Indoor Location System," in *Presented as part of the 10th USENIX Symposium on Networked Systems Design and Implementation (NSDI 13)*, 2013.
- [54] Y. Zhang, B. Wang, H. Zhang, and W. Kong, "True 3D Antenna for UHF RFID Application," in *6th Asia Symposium on Quality Electronic Design (ASQED)*, 2015.
- [55] L. Bolotnyy, S. Krize, and G. Robins, "The Practicality of Multi-Tag RFID Systems," in *IWRT*, 2007.